

Numerical modelling of the triaxial compressive behaviour of closed-cell aluminum alloy foams with computed tomography

J. Zhang¹⁾ and G.P. Zhao²⁾

^{1), 2)} *State Key Laboratory of Mechanical Structure Strength and Vibration,
Xi'an Jiaotong University, Xi'an, 710049, China*

²⁾ zhaogp@mail.xjtu.edu.cn

ABSTRACT

Two three-dimensional (3D) finite element models for the real closed-cell aluminum foam specimen are constructed by employing the microfocus X-ray CT system, 3D reverse reconstruction program and the commercially mesh generation program. The cell wall material properties of closed-cell aluminum foams are precisely determined by comparing the computed uniaxial compressive stress versus strain curve with the measured one in tests. The distributions of stress and strain of cell wall materials are very complicated and unpredictable during the whole compressive deformation process, whilst the mean stresses distribute uniformly along the loading direction. The elastic-plastic constitutive parameters of the cell wall materials are discussed for the influence on the compressive behaviour of closed-cell aluminum foams. By changing the boundary conditions of the foam specimen, various stress states including uniaxial, hydrostatic and proportional loading compression are realized. The crushable foam model with isotropic hardening in ABAQUS and a new constitutive model for foams are verified under triaxial boundary conditions based on these numerical results. The predictions of the new model are more accurate than those of the crushable foam model for triaxial compression.

KEYWORDS: aluminum foams, reverse reconstruction, hydrostatic compression, X-ray CT, constitutive model

1. INTRODUCTION

Closed-cell aluminum foams have been considered as a candidate energy absorption material because of their large deformation at nearly constant plateau stress combined with good heat resistance (Banhart 2001). The compressive behaviour of the foams is dependent on the hydrostatic stress states, and a single uniaxial experimental test is not enough to completely characterize the material behaviour. Many applications of closed-cell aluminum foams lead to a more general state of stress than simple compression or tension. Therefore, Biaxial and triaxial experiments have been conducted on several commercial closed-cell aluminum foams, as shown in Table 1.

¹⁾ PhD student

²⁾ Professor

Table 1. Experimental studies on the multi-axial behaviour of selected commercial closed-cell aluminum foams

Foam type	Stress states	References
Alporas	uniaxial compression/tension, shear, hydrostatic, hydro-compression, biaxial loading	(Andrews et al. 1999), (Gioux et al. 2000), (Deshpande and Fleck 2000), (Doyoyo and Wierzbicki 2003), (Andrews et al. 2001a)
Cymat	uniaxial compression/tension, triaxial compression	(Ruan et al. 2007)
Hydro	uniaxial compression/tension, biaxial loading, hydrostatic	(Doyoyo and Wierzbicki 2003), (Blazy et al. 2004), (Hanssen et al. 2002)
Alulight	uniaxial compression/tension, hydrostatic and hydro-compression	(Sridhar and Fleck 2005), (McCullough et al. 1999)
IFAM	uniaxial compression/tension, torsion, hydrostatic and hydro-compression	(Peroni et al. 2008), (Avalle et al. 2009)
SEU	uniaxial compression/tension, hydrostatic compression and hydro-compression	(Lu and Ong 2001)

The experimental results of closed-cell aluminum foams show noticeable scatter in data. And arbitrary stress states are hardly feasible in experiments. So it is difficult to establish unambiguously the shape of these yield surfaces based on experimental results. Some researchers turn their attention to conduct the mesoscale finite element (FE) models based on a representative volume unit of closed-cell aluminum foams. In general, FE models could be classified into two categories: structural models and discrete models. The structural models are represented by that cellular walls and struts of cellular material are modeled as shell and beam elements, such as Kelvin model (Fischer et al. 2009), cruciform-pyramidal model (Santosa and Wierzbicki 1998), Voronoi tessellation model (Roberts and Garboczi 2001), Gaussian random field model (Roberts and Garboczi 2001), cubic-spherical model (Kim et al. 2006a), ellipsoid-cube model (Czekanski et al. 2005a), ellipsoid-pyramid model (Czekanski et al. 2005b), spheres-triangular model (Gagliardi et al. 2009), random model based on ellipsoidal cells (De Giorgi et al. 2010), truncated cube model (Hasan 2010), cruciform-hemisphere model (Hasan 2010), and tetrakaidecahedra structure model (Nammi et al. 2010). The formulation of shell and beam elements assumes that the longitudinal dimension is much higher than the transversal dimension. This assumption is only valid for low relative density foams, and becomes unreal as density increases. Therefore, beam and shell elements are not suitable for modeling medium-high relative density foams. On the other hand, X-ray tomography has recently emerged as a powerful technique being capable of giving a quantitative description of actual 3D microstructures of cellular materials in a non-destructive way (Elmoutaouakkil et al. 2002; Hangai et al. 2012; Olurin et al. 2002; Singh et al. 2010). The discrete FE models are usually constructed based on

X-ray tomographic data(Bourne et al. 2008; Jeon et al. 2010; Jeon et al. 2009; Michailidis et al. 2008). This method based on virtual foam configuration represents the irregular cell shapes, non-uniform cell wall thickness, unequally geometric distribution and other imperfections of the real foam. The advantage is that the final cellular geometrical body is meshed as a solid element, which steers clear of the defect of shell and beam elements. The only limitation of this type of models is that discretization must be fine enough to properly model continuum structures. It means that the size of elements must be very small and the 3D discrete FE models demand much computational time in practice.

Very few researchers use 3D discrete FE models to investigate the compressive behaviour of closed-cell aluminum foams. Recently, Jeon et al. (Jeon et al. 2009) determined the cell wall mechanical properties of the closed-cell aluminum foam, such as the elastic modulus, 0.2% offset yield stress and power-law hardening exponent, by precisely comparing the computed and measured force versus displacement curves. The effects of each mechanical property on the compressive behaviour of the foam material were also analyzed. The question is that the geometrical dimensions of aluminum foam specimens are taken as a very small cube ($5 \times 5 \times 5 \text{ mm}^3$) including only 2-3 cells in the each direction. Further, Jeon et al.(Jeon et al. 2010) constructed the discrete FE model to explore the detailed deformation and plastic collapse mechanisms of closed-cell aluminum foams under uniaxial compression, and the numerical predictions were compared with the experimentally measured results. However, in their studies, only 5.31% compression strain is calculated, the densification regime is not addressed. Triaxial loading, especially hydrostatic and hydro-compression of closed-cell aluminum foams is still blank in 3D discrete FE analysis.

In this study, two 3D discrete FE models for the real closed-cell Al-Si-Ti alloy foam specimen fabricated via the powder metallurgy foaming technique is constructed by employing the microfocus X-ray CT system, the 3D reconstruction program and the commercially mesh generation program. The cell-wall material properties are precisely determined by comparing the computed uniaxial compressive stress versus strain curves with the measured ones in tests. By changing the boundary conditions of the foam specimen, various stress states including uniaxial, hydrostatic and proportional loading compression are realized for analysis. The crushable foam model with isotropic hardening in ABAQUS and a new foam model are verified under triaxial boundary conditions based on these numerical results.

2. MODELLING OF CLOSED-CELL AL-SI-TI ALLOY FOAMS

The cellular metal investigated in this work is closed-cell Al-Si-Ti alloy foams which are produced using the powder metallurgy foaming technique. The composition of the cell-wall material is Al-7Si (by mass percent) and titanium hydride (TiH_2 , typically 1.0%) which serves as the blowing agent. The fabrication process is similar to that of closed-cell IFAM and Alulight foams. For compression and μCT imaging, two closed-cell Al-Si-Ti alloy foam specimen having relative density of 0.38 and 0.19 are cut in a cube shape with side length 10 and 17 mm(marking as 1# and 2#, respectively). The choice of specimen dimensions insures each specimen has at least 5 cells in the height direction

(Andrews et al. 2001b). An X-ray CT machine (μ CT80, SCANCO Medical AG) is used to characterize the microstructures for two specimen. The 3D scanned data processing software RapidForm (INUS Tech. Inc.) is used to reversely reconstruct the extremely complex structure of two closed-cell Al-Si-Ti alloy foam specimen, as shown in Fig.1. Then, the hexahedron mesh is straightforward generated for the constructed geometric solid models using “body-fitted” mesh method in ANSYS/ICEM. It can be seen in Fig.2 that the mesh size is very small, resulting in the discrete model with up to 250,000 and 500,000 elements for two specimen, respectively. The 3D discrete FE model with so many elements demands much computational time. The further refinements may appreciably improve the accuracy of the calculations, but it seems impossible to resolve in practical times. The commercial explicit finite element code LS-DYNA is employed to carry out all the simulations. Automatic single surface contact options are generally applied to enforce a hard contact between all potentially cell-wall surfaces.

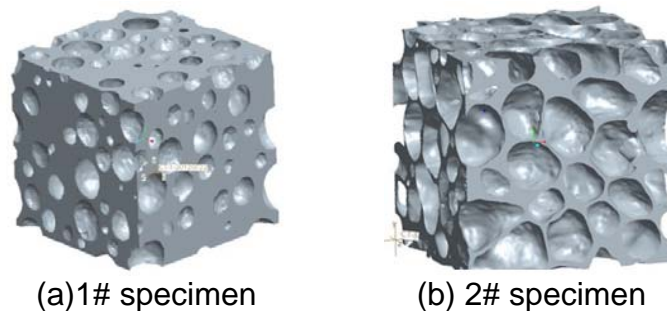


Fig. 1 Geometric solid models for two closed-cell aluminum foam specimen

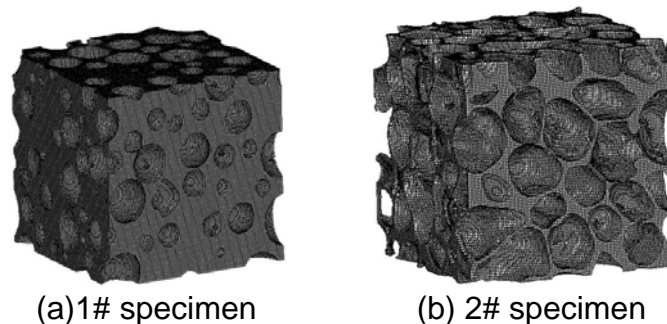


Fig. 2 Computational meshes for two closed-cell aluminum foam specimen

3. CELL WALL MECHANICAL PROPERTIES

The plastic properties of the cell wall material contribute significantly to the mechanical performance of the foam material. However, as the cell wall microstructures are formed differently depending on the production processes and the composition of the cell wall material, measuring the precise values of cell wall material properties has long been a challenge. Campana *et al.* (Campana and Pilone 2008) made 6061, 7075 and Al-7Si specimens which were removed from the outer skins of aluminium foams to

obtain their compressive load versus displacement curves. Hasan *et al.* (Hasan et al. 2008) used the nanoindentation technique for measuring the cell wall mechanical properties (hardness and elastic modulus) of Al-Si-Cu-Mg alloy foams. By inverse modeling of the nanoindentation test and uniaxial compressive test, Kim *et al.* (Kim et al. 2006b) and Jeon *et al.* (Jeon et al. 2009) obtain cell wall material parameters for Al-Si-Cu-Mg alloy foams, Al-Si-Ca alloy foams and Al-Ca alloy foams, respectively.

Using an approach similar to that of Jeon et al. (Jeon et al. 2009), the cell wall material properties of closed-cell aluminum foams are precisely determined by comparing the computed uniaxial compressive stress versus strain curve with that measured experimentally. In simulation of the uniaxial compressive tests, the specimen model is sandwiched between two rigid plates(see Fig.3(a)). The top rigid plate moves downward with a constant velocity while the bottom rigid plate keeps stationary. Its contact edges can slip on both rigid plates with only a slight friction coefficient 0.01, which represents the perfect lubricating condition in experiments. The four side edges of 3D discrete FE model are set free.

Table 2. elastic-plastic constitutive parameters of the cell wall material in LS-DYNA

specimen	elastic modulus (Gpa)	Poisson ratio	yield (MPa)	stress hardening (Gpa)
1#	70	0.3	35	0.06
2#	70	0.3	45	0.03

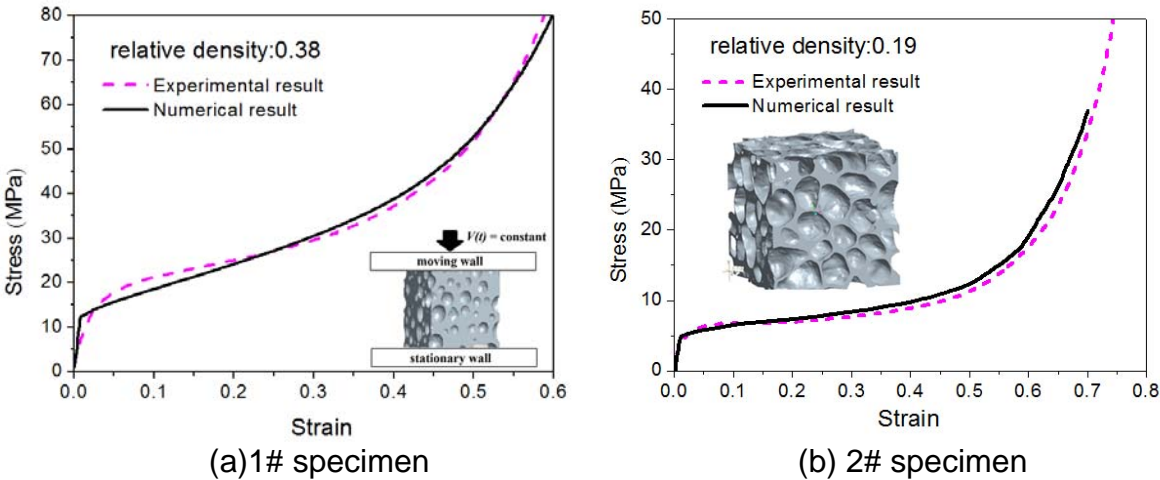


Fig. 3 Numerically predicted and experimentally measured uniaxial compressive deformation process for closed-cell Al-Si-Ti alloy foams

The elastic-plastic constitutive parameters of the cell-wall material are varied to investigate their influence on the compressive behavior of closed-cell aluminum foams. Within the range of the study ,the elastic parameters, such as the elastic modulus and

Poisson ratio, have negligible effects on uniaxial compression stress versus strain curve of closed-cell aluminum foams featured by large deformation. Increasing the yield stress of the cell-wall material considerably increases the magnitude of foam plateau stress, whereas increasing the hardening modulus of the cell-wall material not only increases the magnitude of foam plateau stress, but also reduces foam densification strain. The elastic-plastic constitutive parameters of the cell wall material in LS- DYNA are listed in Table 2. The failure strain is set to 2.0 to prevent excessive deformation of elements, additionally. The numerically predicted and experimentally measured uniaxial compressive deformation and stress versus strain curves of two closed-cell Al-Si-Ti alloy foam specimen are shown in Fig 3. It needs to be highlight that the collapse plateau and densification regimes of the foams are fitted primarily considering their large deformation in practical application. This is different from Jeon *et al.*' study (Jeon et al. 2009) that only linear elasticity and initial plateau regimes are determined.

4. PLASTIC POISSON'S RATIO

The plastic Poisson's ratio ν^p is defined as the negative ratio of the transverse logarithmic strain to the axial logarithmic strain. Due to the volumetric compressibility of aluminum foams, the plastic Poisson's ratio is always smaller than 0.5. It is an important parameter in Zhang's model(Zhang et al. 1998; Zhang et al. 1997), Deshpande and Fleck's model(Deshpande and Fleck 2000),and Miller' model(Miller 2000).However, experimental data of plastic Poisson's ratio seem meagre. Moreover, the available data are too scattered, e.g. the plastic Poisson's ratio of Alporas foam with relative density of 0.08 is 0.33 as reported by Motz et al.(Motz and Pippan 2001), while it is 0.024 by Gioux *et al.* (Gioux et al. 2000).

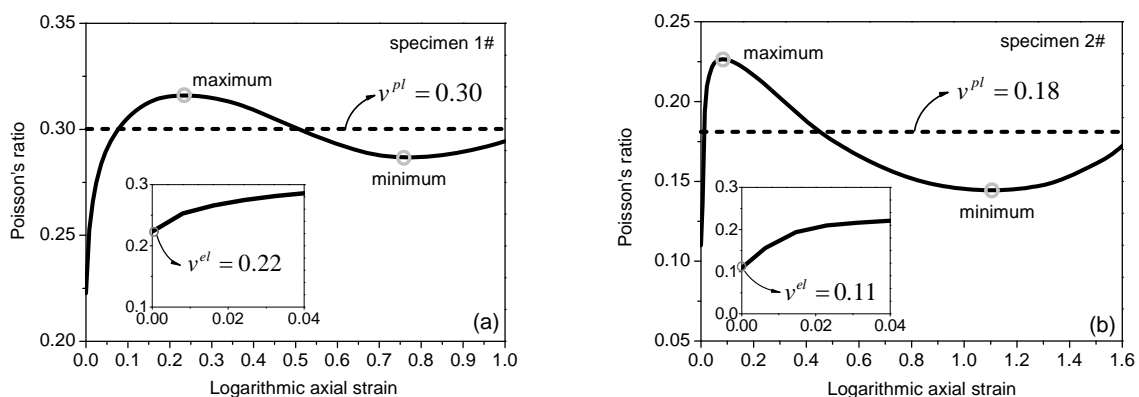


Fig. 4 Numerically predicted plastic Poisson's ratio versus strain curves for closed-cell Al-Si-Ti alloy foams

Theoretically, it is possible to plot the variation of plastic Poisson's ratio versus foam relative density for various foams. We calculate plastic Poisson's ratio of closed-cell

Al-Si-Ti alloy foams using the 3D discrete FE model. The boundary conditions keep the same as that in uniaxial compressive test (see section 3). The only difference is that the each side edges of FE model are set coupled in in-plane displacement respectively, instead of free. Thus the strains in three directions of specimen are measured easily during uniaxial compressive deformation process. Fig. 4 gives the plastic Poisson's ratio versus strain curves and their averages. Note that the plastic Poisson's ratio in two directions obtained from each specimen is fundamentally the same. It can be seen that the plastic Poisson's ratio of each specimen shows a sinusoidal variation as logarithmic axial strain increases. Assuming that the aluminium foams belong to isotropic compressible materials, the average plastic Poisson's ratio may be explored. Additionally, the elastic Poisson's ratio of each specimen can be determined by the initial value of curves.

5. COMPRESSIVE STRESS VERSUS STRAIN CURVES

The uniaxial compressive responses of closed-cell Al-Si-Ti alloy foams are also shown in Fig. 5 based on the numerically results in section 4 using the axes of axial Cauchy stress and logarithmic axial strain.

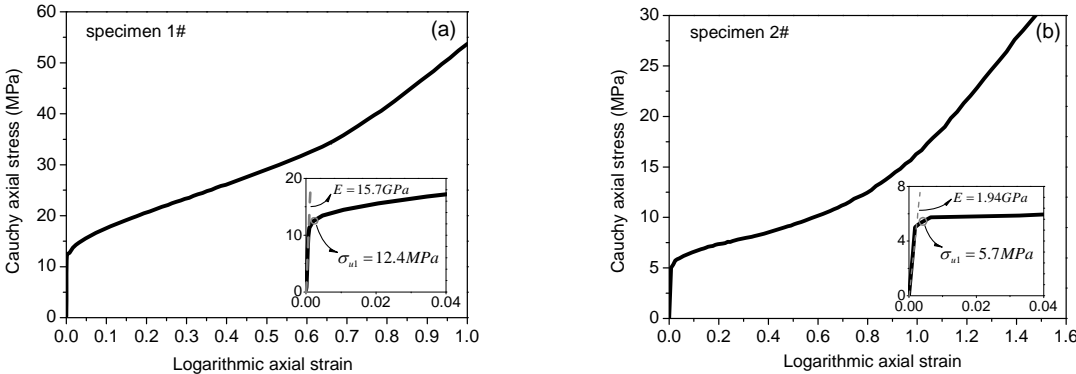


Fig. 5 Numerically predicted axial Cauchy stress versus logarithmic strain curves for closed-cell Al-Si-Ti alloy foams

To simulate the triaxial compression tests, the foam specimen model is sandwiched between six rigid plates. The three rigid plates in different directions move with a same constant velocity toward the opposite stationary ones, respectively. The friction coefficient between contact edges is set to zero. The result from hydrostatic compressive simulation is shown in Fig. 6 via the axes of pressure and logarithmic volumetric strain.

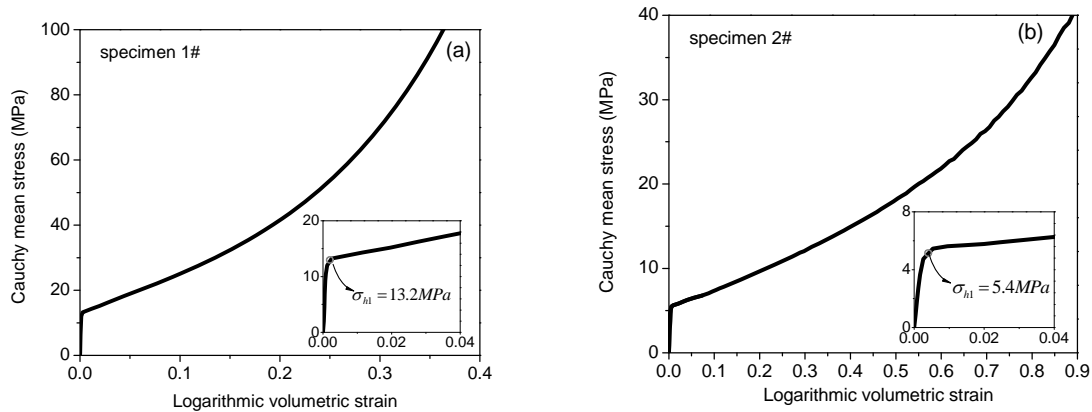


Fig. 6 Numerically predicted hydrostatic compressive stress versus volumetric strain curves for closed-cell Al-Si-Ti alloy foams

A comparison between the hydrostatic and uniaxial compressive stress versus strain curves shows that the hardening rate under hydrostatic compression is much greater than that under uniaxial compression for two specimen. However, in the initial stages of the hydrostatic and uniaxial compression curves, there is little difference between the hydrostatic and uniaxial yield strength.

The 3D discrete FE model is used to investigate the elastic and plastic properties of an open-cell aluminium foam by Wicklein *et al.* (Wicklein and Thoma 2005). Through various combinations of loading velocity in the three directions, various multi-axial stress states are realized in the foam. However, only the elastic regime and the initial yield properties have been analyzed. The proportional compressive loading boundaries in large deformation have not been found in open literatures. To simulate the proportional compression tests, three stationary rigid plates are set to confine displacements of the specimen in three directions, respectively. Three anisotropy elastic surfaces (meshed by solid element), whose out-plane stiffness is much greater than that in in-plane, are set on the opposite surfaces of the specimen. Pressure applied on the surface elements transmits to the foam specimen. Pressure versus time curve is obtained by uniaxial compressive predictions in section 4. Proportional compression loading is realized by

$$\eta = -\frac{\sigma_m}{\sigma_e}$$

changing the pressure factor in three σ directions. The stress ratio σ_m/σ_e is introduced

to define the direction of loading in the $\sigma_e - \sigma_m$ space, with $\eta = 1/3$ denoting for uniaxial compression and $\eta \rightarrow \infty$ for hydrostatic compression. The numerically predicted proportional compressive axial Cauchy stress versus logarithmic strain curves for closed-cell Al-Si-Ti alloy foams are shown in Fig 7.

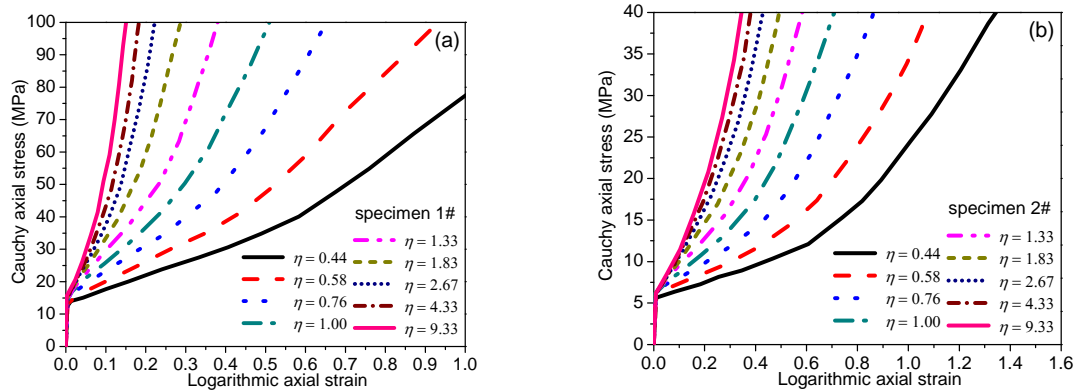


Fig. 7 Numerically predicted proportional compressive axial Cauchy stress versus logarithmic strain curves for closed-cell Al-Si-Ti alloy foams

6. EVOLUTION OF THE YIELD SURFACE

The crushable foam model with isotropic hardening in ABAQUS was originally developed for metallic foams by Deshpande and Fleck (Deshpande and Fleck 2000). The model assumes similar behaviors in tension and compression. The yield surface is an ellipse centered at the origin in the $\sigma_m - \sigma_e$ stress plane and evolves in a self-similar manner governed by the equivalent plastic strain.

The yield surface for the isotropic hardening model is defined as

$$f = \sqrt{\sigma_e^2 + \alpha^2 \sigma_m^2} - B = 0 \quad (1)$$

with

$$\alpha = \frac{k}{\sqrt{1 - \frac{1}{9}k^2}}, \quad k = \frac{\sigma_u^0}{\sigma_h^0} \quad (2)$$

The equivalent plastic strain is defined as

$$\bar{\varepsilon}^{pl} = \sqrt{\left[1 + \left(\frac{\beta}{3}\right)^2\right] \left(\varepsilon_e^2 + \frac{1}{\beta^2} \varepsilon_v^2\right)} \quad (3)$$

The equivalent plastic strain is equal to the absolute value of the axial plastic strain in uniaxial tension or compression. Therefore,

$$B = \frac{1}{3} \sqrt{9 + \alpha^2} \left| \sigma_u(\varepsilon_u^{pl}) \right| \quad (4)$$

The yield surface parameters of two specimen are determined by the numerically predicted results in section 5. Contours of the yield surface are plotted in Fig. 8 in the $\sigma_m - \sigma_e$ space for selected levels of the equivalent plastic strain. It can be seen that the yield surface expands in a self-similar manner. At uniaxial compressive loading path (i.e. $\eta = 1/3$), numerically predicted stress points distribut on the yield surface. However, for hydrostatic compression ($\eta \rightarrow \infty$), numerical and constitutive results show very great differences except the initial yield point.

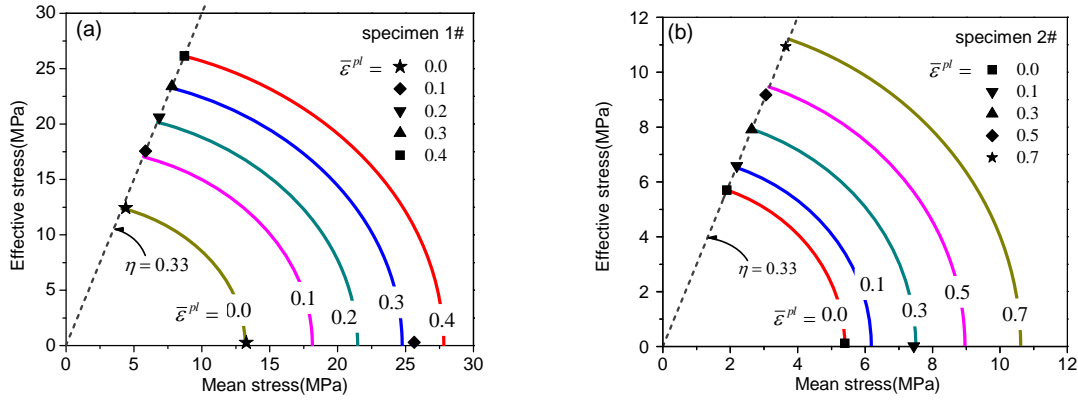


Fig 8. Yield stress surface contours in ABAQUS at selected equivalent plastic levels for closed-cell Al-Si-Ti alloy foams

A new isotropic constitutive model derived from Zhang's model (Zhang et al. 1998; Zhang et al. 1997) is introduced below in order to account for the hydrostatic stress path on the evolution of the yield surface shape.

The yield surface is defined as

$$f = \sqrt{\sigma_e^2 + A(\bar{\epsilon}^{pl})\sigma_m^2} - B(\bar{\epsilon}^{pl}) = 0 \quad (5)$$

with

$$A(\bar{\epsilon}^{pl}) = \sigma_u^2(\bar{\epsilon}^{pl}) / \left(\sigma_h^2(\bar{\epsilon}^{pl}) - \frac{1}{9}\sigma_u^2(\bar{\epsilon}^{pl}) \right) \quad (6)$$

$$B(\bar{\epsilon}^{pl}) = \sigma_h(\bar{\epsilon}^{pl}) \sqrt{\sigma_u^2(\bar{\epsilon}^{pl}) / \left(\sigma_h^2(\bar{\epsilon}^{pl}) - \frac{1}{9}\sigma_u^2(\bar{\epsilon}^{pl}) \right)} \quad (7)$$

Where, $\sigma_u(\bar{\epsilon}^{pl})$ and $\sigma_h(\bar{\epsilon}^{pl})$ are determined from the axial Cauchy stress versus logarithmic strain curves and hydrostatic compressive stress versus volumetric strain curves for closed-cell Al-Si-Ti alloy foams. Specifically, the hydrostatic and shear yield strengths evolve independently .

The equivalent plastic strain $\bar{\varepsilon}^{pl}$ is defined as

$$\bar{\varepsilon}^{pl} = \left| \varepsilon_v^{pl} \right| \quad (8)$$

It can be calculated as below, in the uniaxial and hydrostatic compression respectively

$$\bar{\varepsilon}^{pl} = (1 - 2\nu^{pl}) \left| \varepsilon_u^{pl} \right|, \quad \bar{\varepsilon}^{pl} = \left| \varepsilon_h^{pl} \right|. \quad (9)$$

Determining the new yield surface parameters similarly as above, contours of the new yield surface are plotted in Fig. 9 in the $\sigma_m - \sigma_e$ space for selected levels of the equivalent plastic strain. The present model is calibrated against uniaxial and hydrostatic compression data, and so it agrees with the observed response for these loading paths. what is more, The predictions of this model are in good agreement for intermediate proportional loading path.

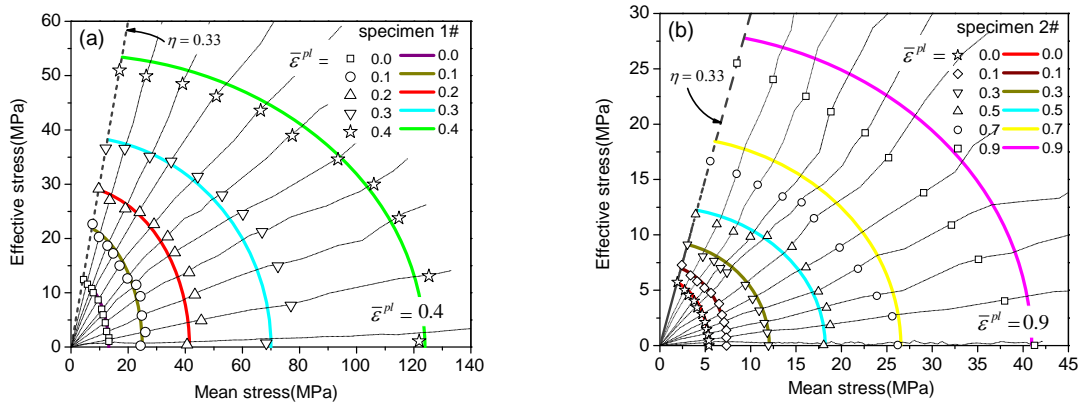


Fig 9. New yield stress surface contours at selected equivalent plastic levels for closed-cell Al-Si-Ti alloy foams

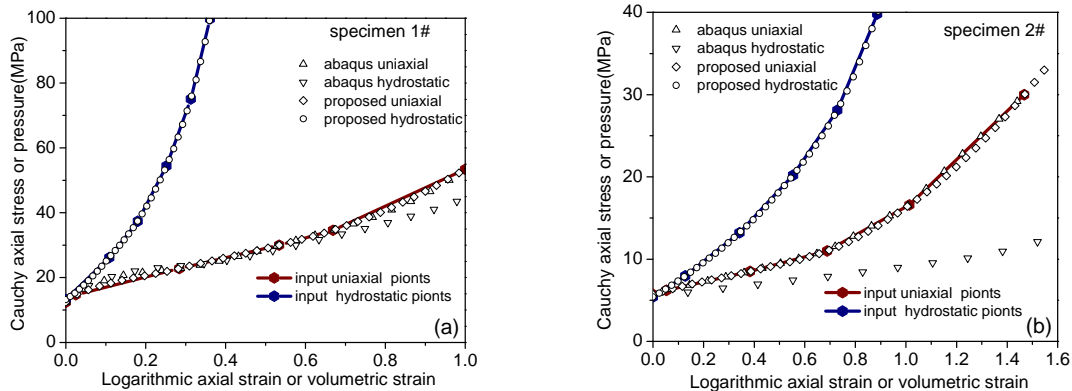


Fig 10. Comparison between stress versus strain curves for closed-cell Al-Si-Ti alloy foams predicted by two yield stress surfaces

In order to show the ability to describe the compressive behavior by two yield surfaces more clearly, Fig 10 shows the uniaxial and hydrostatic compression stress versus strain curves reversely calculated by two yield surface, respectively. The present model is seen to give accurate predictions for both uniaxial and hydrostatic compression. It appears that the crushable foam model with isotropic hardening in ABAQUS substantially undervalues the hydrostatic stress, especially at large strain levels.

To properly validate the new constitutive model, tests other than uniaxial and hydrostatic compression are needed. The related Fortran program of stress update algorithm for this new model including the failure rule is implemented with VUMAT in the commercial software ABAQUS. Verification of the VUAMT program will be presented in later papers.

7. CONCLUSIONS

The triaxial compressive behaviour of closed-cell aluminum foams is investigated numerically. Two 3D FE models for the real closed-cell Al-Si-Ti alloy foam specimen fabricated via the powder metallurgy foaming technique are constructed by employing the microfocus X-ray CT system, the 3D reconstruction program and the commercially mesh generation program. The cell-wall material properties are precisely determined by comparing the computed uniaxial compressive stress versus strain curves with the measured ones in tests. By changing the boundary loading conditions of the foam specimen, various stress states including uniaxial, hydrostatic and proportional compression loading are realized for analysis. The uniaxial, hydrostatic and proportional compression stress versus strain curves for closed-cell Al-Si-Ti alloy foams are predicted numerically. The average plastic Poisson's ratio is also explored in this study. Based on numerical results, the yield surface parameters of the crushable foam model with isotropic hardening in ABAQUS and a new isotropic constitutive model are determined. The present model gives accurate predictions for both uniaxial and hydrostatic compression. Whilst the crushable foam model with isotropic hardening in ABAQUS substantially undervalues the hydrostatic stress, especially at large strain levels.

ACKNOWLEDGEMENTS

This work is supported by the National Basic Research Program of China (2011CB610305), the National Natural Science Foundation of China (11021202) and the Natural Science Foundation of Shaanxi Province (2011JM1012).

REFERENCES

Andrews, E., Sanders, W., and Gibson, L. J. (1999). "Compressive and tensile behaviour of aluminum foams." *Materials Science and Engineering A*, 270, 113-124.

- Andrews, E. W., Gioux, G., Onck, P., and Gibson, L. J. (2001a). "Size effects in ductile cellular solids. Part II: experimental results." *Int J Mech Sci*, 43, 701-713.
- Andrews, E. W., Gioux, G., Onck, P., and Gibson, L. J. (2001b). "Size effects in ductile cellular solids. Part II: experimental results." *INTERNATIONAL JOURNAL OF MECHANICAL SCIENCES*, 43(3), 701-713.
- Avalle, M., Lehmus, D., Peroni, L., Pleteit, H., Schmiechen, P., Belingardi, G., and Busse, M. (2009). "AlSi7 metallic foams - aspects of material modelling for crash analysis." *International Journal of Crashworthiness*, 14(3), 269-285.
- Banhart, J. (2001). "Manufacture, characterisation and application of cellular metals and metal foams." *Prog Mater Sci*, 46(6), 559-632.
- Blazy, J., Marie-Louise, A., Forest, S., and Chastel, Y. (2004). "Deformation and fracture of aluminium foams under proportional and non proportional multi-axial loading: statistical analysis and size effect." *Int J Mech Sci*, 46(2), 217-244.
- Bourne, N. K., Bennett, K., Milne, A. M., MacDonald, S. A., Harrigan, J. J., and Millett, J. C. F. (2008). "The shock response of aluminium foams." *Scripta Mater*, 58, 154-157.
- Campana, F., and Pilone, D. (2008). "Effect of wall microstructure and morphometric parameters on the crush behaviour of Al alloy foams." *Materials Science and Engineering A*, 479, 58-64.
- Czekanski, A., Attia, M. S., Meguid, S. A., and Elbestawi, M. A. (2005a). "On the use of a new cell to model geometric asymmetry of metallic foams." *Finite Elem Anal Des*, 41(13), 1327-1340.
- Czekanski, A., Elbestawi, M. A., and Meguid, S. A. (2005b). "On the FE Modeling of Closed-cell Aluminum Foam." *International Journal of Mechanics and Materials in Design*, 2, 23-34.
- De Giorgi, M., Carofalo, A., Dattoma, V., Nobile, R., Palano, F., Nammi, S. K., Myler, P., and Edwards, G. (2010). "Aluminium foams structural modelling Finite element analysis of closed-cell aluminium foam under quasi-static loading." *Computers and Structures*, 88, 25-35.
- Deshpande, V. S., and Fleck, N. A. (2000). "Isotropic constitutive models for metallic foams." *J Mech Phys Solids*, 48(6-7), 1253-1283.
- Doyoyo, M., and Wierzbicki, T. (2003). "Experimental studies on the yield behavior of ductile and brittle aluminum foams." *Int J Plasticity*, 19(8), 1195-1214.
- Elmoutaouakkil, A., Salvo, L., Maire, E., and Peix, G. (2002). "2D and 3D characterization of metal foams using X-ray tomography." *Adv Eng Mater*, 4(10), 803-807.
- Fischer, F., Lim, G. T., Handge, U. A., and Altstadt, V. (2009). "Numerical Simulation of Mechanical Properties of Cellular Materials Using Computed Tomography Analysis." *J Cell Plast*, 45(5), 441-460.
- Gagliardi, F., De Napoli, L., Filice, L., and Umbrello, D. (2009). "A comparison among FE models to simulate metallic foams forming - An experimental validation." *Mater Design*, 30, 1282-1287.
- Gioux, G., McCormack, T. M., and Gibson, L. J. (2000). "Failure of aluminum foams under multiaxial loads." *Int J Mech Sci*, 42(6), 1097-1117.
- Hangai, Y., Takahashi, K., Yamaguchi, R., Utsunomiy, T., Kitahara, S., Kuwazuru, O., and Yoshikawa, N. (2012). "Nondestructive observation of pore structure deformation behavior of functionallygraded aluminum foam by X-ray computed tomography."

- Materials Science and Engineering A, 556, 678-684.
- Hanssen, A. G., Hopperstad, O. S., Langseth, M., and Ilstad, H. (2002). "Validation of constitutive models applicable to aluminium foams." *Int J Mech Sci*, 44(2), 359-406.
- Hasan, M. A. (2010). "An Improved Model for FEModeling and Simulation of Closed Cell Al-Alloy Foams." *Advances in Materials Science and Engineering*, 1-12.
- Hasan, M. A., Kim, A., and Lee, H. J. (2008). "Measuring the cell wall mechanical properties of Al-alloy foams using the nanoindentation method." *Compos Struct*, 83, 180-188.
- Jeon, I., Asahina, T., Kang, K.-J., Im, S., and Lu, T. J. (2010). "Finite element simulation of the plastic collapse of closed-cell aluminum foams with X-ray computed tomography " *Mech Mater*, 42, 227-236.
- Jeon, I., Katou, K., Sonoda, T., Asahina, T., Kang, K.-J., Buyuk, M., Kan, S., and Loikkanen, M. J. (2009). "Cell wall mechanical properties of closed-cell Al foam." *Mech Mater*, 41, 60-73.
- Kim, A., Tunvir, K., Jeong, G. D., and Cheon, S. S. (2006a). "A multi-cell FE-model for compressive behaviour analysis of heterogeneous Al-alloy foam." *Model Simul Mater Sc*, 14(6), 933-945.
- Kim, A., Tunvir, K., Jeong, G. D., and Cheon, S. S. (2006b). "A multi-cell FE-model for compressive behaviour analysis of heterogeneous Al-alloy foam." *Model Simul Mater Sc*, 14, 933-945.
- Lu, T. J., and Ong, J. M. (2001). "Characterization of close-celled cellular aluminum alloys." *J Mater Sci*, 36(11), 2773-2786
- McCullough, K., Fleck, N., and Ashby, M. (1999). "Uniaxial stress-strain behaviour of aluminium alloy foams." *Acta Mater*, 47(8), 2323-2330.
- Michailidis, N., Stergioudi, F., Omar, H., and Tspas, D. N. (2008). "Investigation of the Mechanical Behavior of Open-Cell Ni Foams by Experimental and FEM Procedures." *Adv Eng Mater*, 10(12), 1122-1126.
- Miller, R. E. (2000). "A continuum plasticity model for the constitutive and indentation behaviour of foamed metals." *Int J Mech Sci*, 42, 729-754.
- Motz, C., and Pippin, R. (2001). "Deformation behaviour of closed-cell aluminium foams in tension." *Acta Mater*, 49(13), 2463-2470.
- Nammi, S. K., Myler, P., and Edwards, G. (2010). "Finite element analysis of closed-cell aluminium foam under quasi-static loading." *Mater Design*, 31(2), 712-722.
- Olurin, O. B., Arnold, M., Korner, C., and Singer, R. F. (2002). "The investigation of morphometric parameters of aluminium foams using micro-computed tomography." *Materials Science and Engineering A*, 328(), 334-343.
- Peroni, L., Avalle, M., and Peroni, M. (2008). "The mechanical behaviour of aluminium foam structures in different loading conditions." *Int J Impact Eng*, 35, 644-658.
- Roberts, A. P., and Garboczi, E. J. (2001). "Elastic moduli of model random three-dimensional closed-cell cellular solids." *Acta Mater*, 49(2), 189-197.
- Ruan, D., Lu, G., Ong, L. S., and Wang, B. (2007). "Triaxial compression of aluminium foams." *Compos Sci Technol*, 67, 1218-1234.
- Santosa, S., and Wierzbicki, T. (1998). "On the modeling of crush behavior of a closed-cell aluminum foam structure." *J Mech Phys Solids*, 46(4), 645-669.
- Singh, R., Lee, P. D., Lindley, T. C., Kohlhauser, C., Hellmich, C., Bram, M., Imwinkelried, T., and Dashwood, R. J. (2010). "Characterization of the deformation

- behavior of intermediate porosity interconnected Ti foams using micro-computed tomography and direct finite element modeling." *Acta Biomaterialia*, 6(6), 2342-2351.
- Sridhar, I., and Fleck, N. A. (2005). "The multiaxial yield behaviour of an aluminium alloy foam." *J Mater Sci*, 40(15), 4005-4008.
- Wicklein, M., and Thoma, K. (2005). "Numerical investigations of the elastic and plastic behaviour of an open-cell aluminium foam." *Materials Science and Engineering A*, 397, 391-399.
- Zhang, J., Kikuchi, N., Li, V., Yee, A., and Nusholtz, G. (1998). "Constitutive modeling of polymeric foam material subjected to dynamic crash loading." *Int J Impact Eng*, 21, 369-386.
- Zhang, J., Lin, Z., Wong, A., Kikuchi, N., Li, V. C., Yee, A. F., and Nusholtz, G. S. (1997). "Constitutive modeling and material characterization of polymeric foams." *J Eng Mater-t Asme*, 119(3), 284-291.